

TEST RESULTS FOR ELECTRON BEAM CHARGING OF
FLEXIBLE INSULATORS AND COMPOSITES

John V. Staskus and Frank L. Berkopce
NASA Lewis Research Center

SUMMARY

This paper discusses the results of materials tests conducted in the Lewis Research Center's geomagnetic-substorm-environment simulation facility. The materials tested were flexible solar-array substrates, graphite-fiber/epoxy - aluminum honeycomb panels, and thin dielectric films. The tests consisted of exposing the samples to monoenergetic electron beams ranging in energy from 2 to 20 keV. Surface potentials, dc currents, and surface discharges were the primary data.

Four solar-array substrate samples were tested. These samples consisted of Kapton sheet reinforced with fabrics of woven glass or carbon fibers. They represented different construction techniques that might be used to reduce the charge accumulation on the array back surface.

Five honeycomb-panel samples were tested, two of which were representative of Voyager antenna materials and had either conductive or nonconductive painted surfaces. A third sample was of Navstar solar-array substrate material. The other two samples were of materials proposed for use on Intelsat V. All the honeycomb-panel samples had graphite-fiber/epoxy composite face sheets.

The thin dielectric films were 2.54-micrometer-thick Mylar and 7.62-micrometer-thick Kapton.

INTRODUCTION

Many geosynchronous satellites have experienced behavior anomalies in electronics systems at some time during their lifetimes (refs. 1 and 2). These anomalies are believed to result from discharges that take place on various satellite surfaces after differential charging by the geomagnetic substorm environment (ref. 3). The Lewis Research Center has undertaken investigations of the charging behavior of various materials in its geomagnetic-substorm-environment simulation facility (ref. 4). Thermal control materials and some solar-array segments have undergone considerable testing (refs. 5 to 7). Concern about the behavior of materials proposed for use on future satellites led to the testing of several flexible insulator and composite samples.

Flexible-substrate solar arrays used on some communications satellites present a large insulator area that can be charged by the environment. The

first such array was designed and built for the Canadian-American Communications Technology Satellite (CTS) before spacecraft charging effects were understood. However, there was sufficient concern for the possible charging of this array that a charging investigation was conducted (ref. 8). The CTS has survived environmental charging since its launch in January 1976 but has suffered a power loss possibly because of a charging event (ref. 9).

When a similar solar array was proposed for use on the latest Comsat satellite, Intelsat V, several modifications to the substrate were suggested to minimize the charging of the dielectric surface. The Kapton-fiberglass substrate was changed to include woven carbon-fiber fabrics, or conductive surface coatings, or both. The fabric and coatings would be electrically grounded. These "quasi-conductive" dielectric substrates required testing to evaluate their effectiveness in controlling surface charging. Four solar-array segments with different carbon-fabric weaves and surface coatings were prepared by AEG-Telefunken and Comsat Corp. These segments are part of the samples tested and reported on herein.

Five graphite-fiber/epoxy - aluminum honeycomb panels (samples of materials for the Navstar, Voyager, and Intelsat V satellites) were also tested. They are representative of solar-array substrates, antenna materials, and structural panels used on these satellites. The two antenna-panel samples were painted, one with a conductive paint and the other with a nonconductive paint.

Two thin-film materials, 2.54-micrometer-thick aluminized Mylar and 7.62-micrometer-thick Kapton, were also tested.

The flexible-substrate solar-array samples and the Intelsat V honeycomb-panel samples were furnished by the Comsat Corp. The Navstar honeycomb-panel sample was provided by the Rockwell International Corp. And the Voyager honeycomb-panel samples were supplied by the Jet Propulsion Laboratory.

DESCRIPTIONS OF SAMPLES

Flexible-Substrate Solar-Array Samples

The four flexible-substrate solar-array samples were nominally 10 centimeters by 11 centimeters in area. The substrates were made of 12.5-micrometer-thick Kapton sheet (density, 19 g/m²) that was reinforced with either a woven carbon-fiber material or a woven glass-fiber material bonded to one surface. A silver-filled polyester strip bonded to the back surface along each 10-centimeter edge provided electrical contact to the reinforcing and/or charge-control material. The front surface of each sample held 2-centimeter-by-4-centimeter solar cells of 10-ohm-centimeter resistivity.

Sample 1 (fig. 1) had 66-g/m² woven carbon-fiber material bonded to the back surface for reinforcing and charge control. The fabric elements were approximately 0.15 centimeter wide and were spaced 5 per centimeter, resulting in a bare Kapton area of about 6 percent. The conductive polyester edge-strips

were spaced 10 centimeters apart with 50 carbon-fabric elements connecting them. The woven material contained 48 carbon-fabric elements crossing the sample parallel to the polyester edge-strips. A short piece of Kapton-insulated wire was bonded into each polyester strip for making circuit connections. The resistance across the back of the substrate was 3.6 ohms. Eight 2-centimeter-by-4-centimeter solar cells were mounted on the bare Kapton front surface of the substrate in two parallel strings of four cells in series. The 0.01-centimeter-thick cerium-doped cover slides were applied with DC 9350 adhesive and were similar to those used on the Communications Technology Satellite (ref. 8).

Sample 2 (fig. 1) had 45-g/m² woven carbon-fiber reinforcing and charge-control material bonded to the back surface. The fabric elements were about 0.1 centimeter wide and were spaced approximately 3½ per centimeter, resulting in a bare Kapton area of about 42 percent. The conductive edge-strips were 9.8 centimeters apart and were joined by 34 carbon-fabric elements. Thirty-two carbon-fabric elements crossed the substrate parallel to the conductive edge-strips. The resistance of the substrate between the strips was 3.9 ohms. Circuit connections to the strips were made through a short piece of silver mesh bonded into each strip. Four 2-centimeter-by-4-centimeter solar cells connected in series were attached to the bare Kapton surface of the substrate. The long dimensions of the substrate and the cells were parallel. The 0.015-centimeter-thick cerium-doped cover slides had a magnesium fluoride antireflection coating.

Sample 3 (fig. 1) was like sample 2 except that a film of soot-bearing adhesive was spread over the woven carbon-fabric material to cover the bare Kapton and to improve the conductivity of the back surface. Thirty-three strands of the carbon-fabric material crossed the sample perpendicular to the conductive edge-strips, which were 9.9 centimeters apart. Thirty-two strands of material crossed the substrate parallel to the conductive edge-strips. Substrate resistance between the conductive edge-strips was 2 ohms.

Sample 4 (fig. 1) had 27-g/m²-dense woven glass-fiber material applied to the front surface of the substrate for reinforcing. The weave density of about 24 strands per centimeter allowed very little, if any, bare Kapton to be exposed. Soot-bearing adhesive, as used on sample 3, was applied to the bare Kapton on the back surface. Two conductive polyester edge-strips were placed 9.9 centimeters apart on top of the soot-bearing adhesive. The resistance of the substrate between the strips was 5.3 kilohms. Table I summarizes the sample characteristics.

Graphite-Fiber/Epoxy - Aluminum Honeycomb Samples

Five honeycomb-panel samples were tested. All five had aluminum honeycomb cores with graphite-fiber/epoxy face sheets. Two of the samples were painted, one with a conductive paint and the other with a nonconductive paint. The remaining three samples had bare graphite-fiber/epoxy face sheets. The largest specimen (sample 5) was a sample of the Navstar satellite solar-array substrate. It was 30.8 centimeters by 29 centimeters by 1.59 centimeters thick.

Its 0.03-centimeter-thick face sheets were wrapped around two opposite edges of the core and were joined, making a loop around the core. A gap in the graphite-fiber material ran halfway around the loop across one face of the sample. The epoxy content was higher along this stripe than over the rest of the face sheet.

The two painted samples (6 and 7) were Voyager satellite antenna materials. The nonconductive painted sample was 38 centimeters by 6 centimeters by 1.6 centimeters thick with PV100 (titanium oxide in silicone alkyd) paint on one surface. The sample with conductive paint (7) was 14 centimeters by 14 centimeters by 2.5 centimeters thick with Goddard Space Flight Center paint designated NS43C on both sides.

The remaining two honeycomb-panel specimens (8 and 9) were samples of materials proposed for use on the Intelsat V satellite. Both specimens were 15 centimeters square. Sample 8 had 0.01-centimeter-thick woven graphite-fiber/epoxy face sheets bonded to a 1.8-centimeter-thick aluminum honeycomb core with 0.005 centimeter of unsupported epoxy. Sample 9 had 0.04-centimeter-thick unidirectional graphite-fiber/epoxy face sheets bonded to a 0.86-centimeter-thick aluminum honeycomb core. Both samples had a hole drilled through one corner. An aluminum block was cemented in the hole with conductive adhesive. The block provided a point for mounting and for making electrical connections.

Thin-Film Samples

The thin-film materials tested were

- (1) Kapton polyimide film - type H, 127 micrometers thick and with a vapor-deposited aluminum film on one side
- (2) Kapton polyimide film - type H, 7.62 micrometers thick and uncoated
- (3) Mylar polyester film, 2.54 micrometers thick and with a vapor-deposited aluminum film on one side

The two thinner films were tested both totally isolated from ground and mounted on a grounded substrate. The thickest material was tested only while mounted on a grounded substrate.

The aluminum substrates were 17.1 centimeters by 20.3 centimeters with leads attached for measuring charging and leakage current. The two aluminized films were mounted with the aluminized sides in contact with the substrates. The two thinner films were mounted by wrapping the film around the substrate edges and taping it to the substrate back.

DISCUSSION OF TESTS AND RESULTS

Flexible-Substrate Solar-Array Samples

The testing of the flexible-substrate solar-array samples consisted of three parts. In the first part, the front surfaces were exposed to monoenergetic electron beams of 2 to 20 keV while in total darkness. In the second part, the back surfaces were exposed to monoenergetic electron beams while in total darkness. In the third part, the front surfaces were simultaneously exposed to a 20-keV electron beam and simulated solar illumination. The intensity of the illumination at the experiment surface was approximately 0.6 times the solar intensity at 1 AU. Nominal electron flux was 1 nA/cm^2 for all tests.

Each test was begun with the sample surface neutral. A gaseous-nitrogen ion source was used between tests to discharge this surface. During the tests, electron current collected by the solar cells and that collected by the substrate were monitored separately. The sample's surface potential was monitored with a noncontact, field-nulling, electrostatic voltmeter whose probe could be swept across the surface at a separation of about 0.2 centimeter. Discharge activity was monitored with a 15-centimeter-diameter loop antenna centered about 38 centimeters from the sample center.

The first series of tests - run for 20 to 30 minutes at beam voltages of 2, 5, 8, 10, 12, 14, 16, 18, and 20 kilovolts - were conducted to survey the response of the substrate front surface and the solar-cell cover slides. The second series of tests - run for 20 to 30 minutes at beam voltages of 2, 8, 12, 16, and 20 kilovolts - were conducted to survey the response of the back surface. The test results were compared to determine the most effective technique for controlling charge buildup on the back surfaces. In the third series of tests, the front surface of each sample was irradiated with a 1-nA/cm^2 , 20-keV electron flux for 2 hours. The first 1/2 hour of the test was like the initial front-surface tests except that the sample temperature was lowered to about -18°C . During the second 1/2 hour the sample was illuminated by a solar simulator that produced about 0.6 times 1-AU solar intensity at the sample plane. During the third 1/2 hour the sample was again in darkness, and during the fourth 1/2 hour it was again illuminated. Throughout the test the temperature, substrate collection current, cell-circuit collection current, and surface potential profile were recorded each minute. During the illuminated portions of the test, the array-segment short-circuit current and open-circuit voltage was also recorded each minute.

The test results for sample 2 are shown in figures 2 to 5. Figure 2 shows typical surface potential profiles for the front and back surfaces of the sample taken while the surfaces were being bombarded in darkness. Figures 2(a) and (b) are equilibrium profiles of the front surface under exposure to 5-keV (low energy) and 20-keV (high energy) beams, respectively. The low-energy beam charges the Kapton border to a significantly higher potential than the solar-cell cover slide. The high-energy beam charges the cover slide and the Kapton border to comparable potentials. Figures 2(c) and (d) show the back surface in a high-energy beam early in the test and at equilibrium. The

approximately 0.1-centimeter-wide carbon-fiber threads and the intervening 0.2-centimeter squares of Kapton are resolvable as the alternating potential peaks and valleys. The conductive strips on the sample edges show up as high potential peaks. The most significant observation to be made is that the small open areas of Kapton on the back surface become charged to nearly the same potential as the broad open Kapton borders on the front surface.

Figure 3 shows the range of potentials occupied by the various surface materials of the sample for exposure to 2- to 20-keV electron beams. Figure 4 shows the equilibrium electron currents to the conductive substrate and solar-cell circuits in 2- to 20-keV electron beams. The current collected by the solar-cell circuit during electron irradiation of the back surface is not shown since it was more than an order of magnitude less than the current collected during front-surface irradiation.

The test conducted with the solar simulator is summarized in figure 5. Figures 5(a) and (b) show the surface potentials on the cover slides and the Kapton substrate border. Under illumination of only 0.6 Sun intensity, the surface potentials are reduced by an order of magnitude from the values reached during electron irradiation in total darkness possibly because of the photoconductivity of Kapton (ref. 10). Figure 5(c) shows sample temperature as a function of time. The thermocouple used to monitor the temperature was located in the center of the substrate's back surface. Because of its location it probably indicated the true temperature of all the sample surfaces only during the first 1/2 hour of testing. During this time, there were no thermal inputs to the sample and a steady state had been achieved. Figure 5(d) is a cumulative record of the discharge activity that took place during the test. The three counters connected to the loop antenna were operating with thresholds of 1, 2, and 5 volts. The top curve shows the discharges that generated pulses greater than 1 volt in the antenna. The bottom curve shows discharges that induced pulses greater than 2 volts. No discharges generating 5 volts were observed during the 2-hour test of sample 2. Discharge activity was greatest during the first 1/2 hour when the sample was cold and in darkness. The discharge rate was reduced after illumination of the sample but increased during the second 1/2 hour of darkness. The discharge rate during the second dark period was somewhat less than the rate during the first dark period possibly because of higher sample temperature.

The test results obtained with sample 3 are shown in figures 6 to 9. Figure 6 shows typical potential profiles for this sample. Sample 3 was identical to sample 2 except for the addition of the soot-bearing adhesive charge-control material to the back surface. The cover-slide and Kapton-border potential profile for low-energy (5-keV) electron beam irradiation (fig. 6(a)) is very similar to that for sample 2 (fig. 2(a)). The profile for high-energy (20-keV) electron beam irradiation (fig. 6(b)) shows that the Kapton border became less highly charged probably because of the additional soot-bearing adhesive charge-control material. The most dramatic improvement is shown in figure 6(c), the profile of the back surface exposed to a 20-keV electron beam. The maximum potential is two orders of magnitude less than that of the sample without the adhesive-soot material (sample 2). Figures 7 to 9 show surface potential as a function of beam energy, collected electron current as a function of beam

energy, and the curves summarizing the 2-hour test in which the sample was illuminated by simulated solar radiation.

The test results for sample 4 are summarized in figures 10 to 13. Figure 10(a) shows the potential profile of the front surface under exposure to a low-energy (5-keV) electron beam. The cover slide and the fiberglass-over-Kapton border became charged to approximately the same potentials as the cover slides and Kapton borders of samples 2 and 3. The potential profile of the front surface under exposure to a high-energy (20-keV) electron beam is shown in figure 10(b). Exposure of the back surface to a 20-keV beam produced the potential profile shown in figure 10(c). Recall that the back surface has the soot-bearing charge-control material applied to plain Kapton without any woven carbon-fiber material. Comparison with figure 6(c) shows that the adhesive-soot material alone is nearly as effective as the combined woven-carbon-fiber and adhesive-soot material in reducing charge accumulation. Figures 11 to 13 show surface potential as a function of beam energy, collected electron current as a function of beam energy, and the curves summarizing the 2-hour test of the sample subjected to alternating periods of darkness and simulated solar illumination.

The test results for sample 1 are summarized in figures 14 to 17. This sample was a better simulation of a proposed flight array in that the exposed area of the substrate on the solar-cell side was a small fraction of the total sample area. Figure 14(a) shows the two deep potential wells due to charge accumulation on the narrow Kapton borders. The potentials reached by the surfaces in the low-energy (5-keV) electron beam were much the same as the levels reached by similar surfaces on the other three samples. The voltage probe crossed four solar-cell cover slides as it traversed the sample, and evidence of these is barely discernible in figure 14(a). Figure 14(b) is a typical surface potential profile of sample 1 in a high-energy (20-keV) electron beam. The cover slides are more easily seen. The potential profile of the back surface in a 20-keV electron beam is shown in figure 14(c). The back surface of this sample looks much like the back surface of sample 2, except that the carbon-fiber material is more densely woven. Comparing figure 14(c) with figure 2(c) shows that the closer weave eliminated the numerous highly charged regions evident on the back-surface profile of sample 2. Although an improvement over the behavior of sample 2 was realized, the closer weave was not as effective in reducing charge accumulation as the adhesive-soot material applied to samples 3 and 4 (figs. 6(c) and 10(c)). Figures 15 to 17 show surface potential as a function of beam energy, sample current as a function of beam energy, and the curves summarizing the 2-hour test with periods of solar simulation.

Sample 1 experienced significantly more discharge activity on the front surface than did the other three samples. This may be due to the larger number of solar cells, whose cover slides could become charged and independently discharge to the solar-cell interconnections. Comparing figures 5(d), 9(d), 13(d), and 17(d) shows that illumination of the front surface significantly reduced or eliminated discharge activity on all samples, possibly because of the photoconductivity of Kapton (ref. 10). The data indicate that the densely woven carbon-fiber fabric alone or the less-dense carbon-fiber fabric with the

adhesive-soot material added were most effective in preventing discharge activity when the back surface was irradiated in darkness.

Graphite-Fiber/Epoxy - Aluminium Honeycomb Samples

The five honeycomb-panel samples were tested to determine, in each case, the degree to which the surfaces of interest became charged in monoenergetic electron beams of 2 to 20 keV.

The Navstar sample (5) was mounted with its back surface against a 27.3-centimeter-by-29.3-centimeter aluminum plate to which a lead was attached to measure electron current to the sample. Typical surface potential profiles are shown in figure 18(a). The ragged profile is probably a result of variation in the concentration of epoxy and graphite fibers at the surface. Note the prominent potential spike at the discontinuity in the graphite-fiber sheet. The general surface potential across the sample is shown in figure 18(b) as a function of beam energy. For energies greater than 5 keV, the potential increases only slightly if at all. The nominal current density at the center of the sample was 1 nA/cm² before each test, as read by the Faraday cup. The sample current recorded for each test was nearly 1 microampere, indicating an average flux over the 893-square-centimeter sample of about 1 nA/cm². No discharges were recorded by the loop antenna located near the sample or by the time-exposure camera.

The Voyager antenna samples (6 and 7) were exposed to electron beams of 2 to 20 keV and flux densities of 1 and 3 nA/cm². The dependence of the surface potential on beam energy and flux density is shown in figures 19(a) and (b). The dependence on beam energy disappears or is much reduced above 10 keV for both samples. The surface potential of the conductive-paint sample is about two orders of magnitude lower than that of the nonconductive-paint sample for the same beam conditions. Data from earlier tests of another nonconductive paint (S-13G10) is shown in figure 19(c) for comparison.

The sample 8 and 9 honeycomb-panel surfaces were also exposed to 2- to 20-keV electron beams of 1- to 3-nA/cm² flux density. The samples were tested simultaneously, side by side. The tests were conducted with the samples at -40° C to better simulate the environment of the materials in use on Intelsat V. Typical surface potential profiles are shown in figure 20(a). The results of these tests, including the Navstar test data for comparison, are shown in figure 20(b). The ragged appearance of sample 8's profiles is similar to the Navstar profiles and is probably due to the varying epoxy concentration across the surface. Sample 9's profiles appear more uniform, with two prominent potential spikes at the locations of significant epoxy bleed through the carbon fibers. Though the loop antenna did not record any discharge activity, the sample current record and the time-exposure photographs show evidence of activity on sample 8.

The sample current records (fig. 21(a)) were quite noisy. The pulses on sample 9's current record may have been a response to what was happening on the other sample. The time-exposure photographs (fig. 22) show a faint glow out-

lining the graphite-fiber pattern of sample 8 but show no evidence of discharges from sample 9. Also, the surface potential of sample 8 appeared different with each sweep of the probe (fig. 21(b)), but sample 9's profile appeared nearly constant.

Thin-Film Samples

The first test specimen of Mylar was about 28 centimeters square and was isolated from ground, with the bare surface facing the electron source. An electron beam of nominally 1 nA/cm^2 , at its center, in the plane of the specimen was stepped through various energies from $2\frac{1}{2}$ to 20 keV. The potential of the Mylar surface was monitored by the electrostatic voltmeter.

The response of surface potential of the Mylar film to the varying beam energy is shown in figure 23. With the specimen isolated from ground and in total darkness, thus eliminating bulk conduction and photoemission currents, the equilibrium surface potential was a function of beam energy and the material secondary emission properties. Although no temperature-measuring devices were mounted on the specimen, it was estimated that the specimen was at 10° C , as were other structures within the chamber.

The surface potential response of the 7.62-micrometer-thick Kapton film to varying beam energy, with the specimen totally isolated from ground, is shown in figure 24. In this configuration, the surface potential is about the same as that of the Mylar film mounted similarly and exposed to the same-energy electron beam. The surface potentials are compared in figure 25 as a function of beam energy for both materials in the totally isolated and grounded substrate mounting configurations. The test data and calculated values of resistance and resistivity are contained in table II.

The data from the testing of the 127-micrometer-thick Kapton film show that the surface potential increased linearly with beam energy to about 12 keV. Beyond this level, discharges began to take place on the surface. The data taken were not sufficient to tell whether the discharges were characterized by charge transport from the front surface to the back surface at the edges or by charge emission from the surface to other structures within the chamber.

CONCLUSIONS

Four flexible-substrate solar-array segments, five graphite-fiber/epoxy - aluminum honeycomb panels, and two thin dielectric films were exposed to monoenergetic electron beams in the Lewis Research Center's geomagnetic-substorm-environment simulation facility. The array segments represented different approaches to making the dielectric back surface "quasi-conductive" and thus minimizing surface charge accumulation. The tests showed, as expected, that the more nearly continuous the quasi-conductive surface treatment, the lower the surface potential. The tests of the honeycomb-panel samples are evidence that strong, lightweight, nonmetallic structural materials are available that

have acceptable spacecraft-charging properties. If the surfaces have a sufficiently high and uniform concentration of conductive medium with a conductive path to ground, surface potentials well below those at which discharges occur can be maintained. Finally, thin dielectric films charge to high surface potentials when they are isolated from ground. However, when the films are placed over a conductive substrate at ground potential, surface potentials of less than 2½ kilovolts can be maintained even when the films are irradiated with 20-keV electrons.

REFERENCES

1. Fredricks, R. W.; and Scarf, F. L.: Observation of Spacecraft Charging Effects in Energetic Plasma Regions. Photon & Particle Interactions with Surfaces in Space, R. J. L. Garard, ed., D. Reidel Publ. Co., 1973, pp. 277-308.
2. McPherson, D. A.; Cauffman, D. P.; and Schober, W. R.: Spacecraft Charging at High Altitudes: The SCATHA Satellite Program. AIAA Paper 75-92, Jan. 1975.
3. Rosen, A.: Spacecraft Charging - Environment Induced Anomalies - Magnetic Substorm Effects. AIAA Paper 75-91, Jan. 1975.
4. Berkopéc, Frank D.; Stevens, N. John; and Sturman, John C.: The Lewis Research Center Geomagnetic Substorm Simulation Facility. NASA TM X-73602, 1976.
5. Stevens, N. John; Klinect, Vernon W.; and Berkopéc, Frank D.: Environmental Charging of Spacecraft Surfaces: Tests of Thermal Control Materials for Use on the Global Positioning System Flight Space Vehicle, Part 1: Specimens 1-5. NASA TM X-73467, 1976.
6. Stevens, N. John; Berkopéc, Frank D.; and Blech, Richard A.: Environmental Charging of Spacecraft Surfaces: Tests of Thermal Control Materials for Use on the Global Positioning System Flight Space Vehicle, Part 2: Specimens 6-9. NASA TM X-73436, 1976.
7. Stevens, N. John; et al.: Testing of Typical Spacecraft Materials in a Simulated Substorm Environment. NASA TM X-73603, 1976.
8. Stevens, N. John; Lovell, Robert R.; and Gore, J. Victor: Spacecraft Charging Investigation for the CTS Project. NASA TM X-71795, 1975.
9. Stevens, N. John; Klinect, Vernon W.; and Gore, J. Victor: Summary of CTS Transient Event Counter Data After One Year of Operation. NASA TM X-73710, 1977.
10. Coffey, H. T.; Jenevics, J. E.; and Adamo, R. C.: Photoconductivity of High-Voltage Space Insulating Materials. (SRI Proj. 3545, Stanford Res. Inst.; NASA Contract NAS3-18912.) NASA CR-134995, 1975.

TABLE I. - SAMPLE SUBSTRATE CHARACTERISTICS

Sample	Materials ^a	Element	Substrate without anticharging	Dimensions, mm	Anticharging represented by-	Resistance between conductive edge-strips ^a k Ω
		Density, g/m ²				
1	Kapton (12.5 μ m) CFC ^b CY 209 plus hardener HT 972	19 66 66	155	100 x 110	CFC ^b	0.0036
2	Kapton (12.5 μ m) CFC ^b DuPont 46971 plus hardener RC 805	19 45 31	95	100 x 110	CFC ^b	0.0039
3	Kapton (12.5 μ m) CFC ^b DuPont 46971 plus hardener RC 805	19 45 40	104	100 x 110	CFC, ^b DuPont 46971, hardener, and soot	0.0020
4	Kapton (12.5 μ m) Fiberglass 90001 DuPont 46971 plus hardener RC 805	19 27 13	59	100 x 110	DuPont 46971, hardener, and soot	5.297

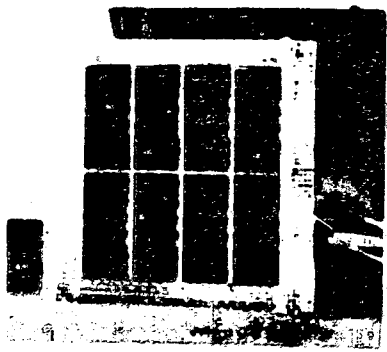
^aAll the samples had two strips of silver-filled polyester bonded to the back surface so that the back surface could be grounded.

^bCarbon-fiber composite.

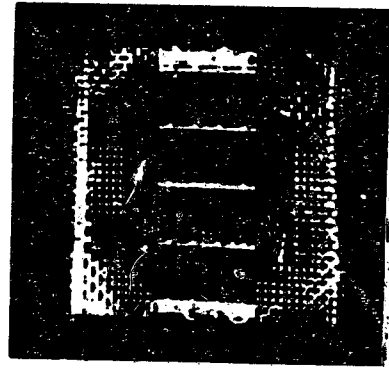
TABLE II. - TEST DATA AND CALCULATED RESISTANCE FOR THIN PLASTIC FILMS

Sample	Beam energy, keV	Surface potential, kV	Beam voltage minus surface voltage, kV	Sample current, μ A	Sample current divided by area, nA/cm ²	Effective bulk resistance, Ω	Effective bulk resistivity, Ω -cm
127- μ m-thick Kapton	2.5	1.64	0.86	0.011	0.032	0.149×10^{12}	0.409×10^{16}
	5	4.15	.85	.005	.014	$.83 \times 10^{12}$	2.277×10^{16}
	8	7	1	.006	.017	1.167×10^{12}	3.201×10^{16}
	10	9.0	1	.005	.015	1.8×10^{12}	4.938×10^{16}
	12	10.8	1.2	.007	.020	1.543×10^{12}	4.232×10^{16}
	^a 15	12.8	2.2	.008	.023	1.6×10^{12}	4.389×10^{16}
	^a 18	12.8	5.2	.012	.035	1.067×10^{12}	2.927×10^{16}
^a 20	13.0	7	.013	.037	1×10^{12}	2.743×10^{16}	
7.62- μ m-thick Kapton	2.5	1.63	0.87	0.028	0.08	5.82×10^{10}	2.662×10^{16}
	5	2.12	2.88	.229	.657	$.926 \times 10^{10}$	$.423 \times 10^{16}$
	8	2.10	5.90	.278	.798	$.755 \times 10^{10}$	$.345 \times 10^{16}$
	10	1.96	8.04	.298	.823	$.658 \times 10^{10}$	$.300 \times 10^{16}$
	15	1.20	13.8	.579	1.66	$.207 \times 10^{10}$	$.094 \times 10^{16}$
	20	.50	19.5	.340	.978	$.147 \times 10^{10}$	$.067 \times 10^{16}$
2.54- μ m-thick Mylar	2.5	1.1	1.4	0.09	0.259	1.222×10^{10}	1.676×10^{16}
	5	.925	4.075	.191	.548	$.484 \times 10^{10}$	$.664 \times 10^{16}$
	10	.32	9.68	.322	.924	$.099 \times 10^{10}$	$.136 \times 10^{16}$
	20	.039	19.961	.380	1.11	$.01 \times 10^{10}$	$.014 \times 10^{16}$

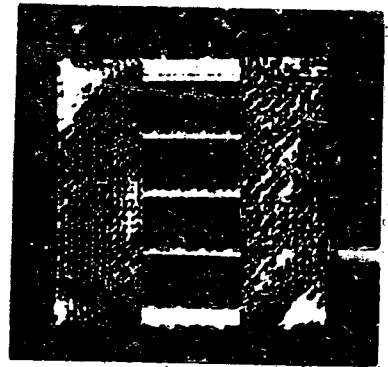
^aSurface discharges occur; surface potential not truly in equilibrium; all samples 17.04 cm by 20.32 cm.



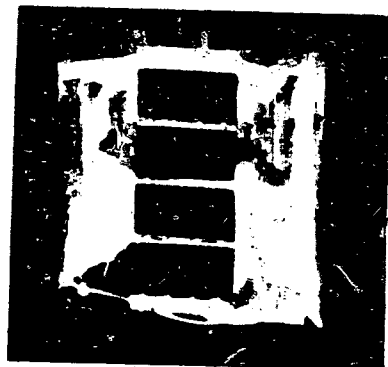
Front surface



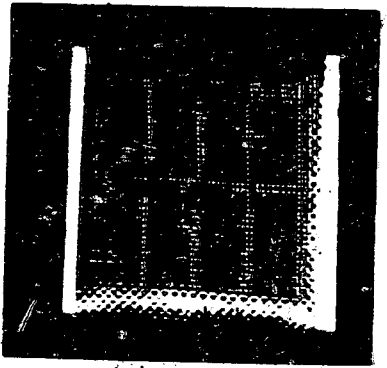
Front surface



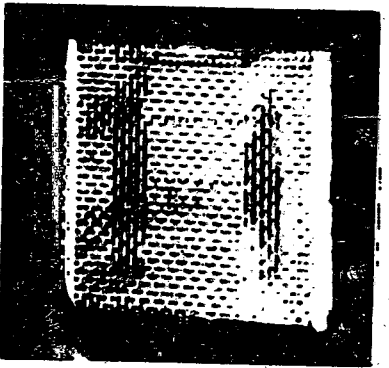
Front surface



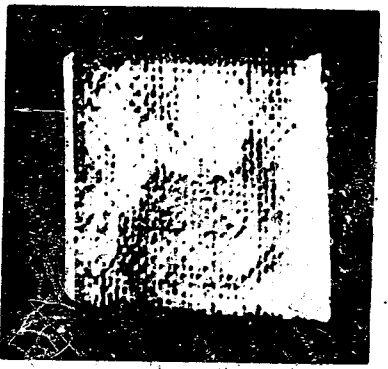
Front surface



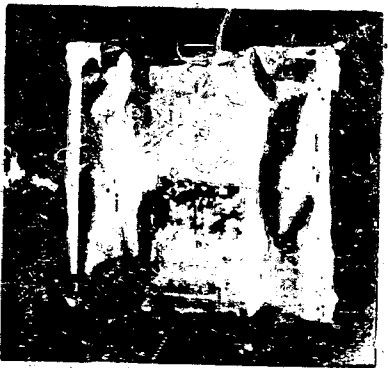
Back surface
(a) Sample 1.



Back surface
(b) Sample 2.

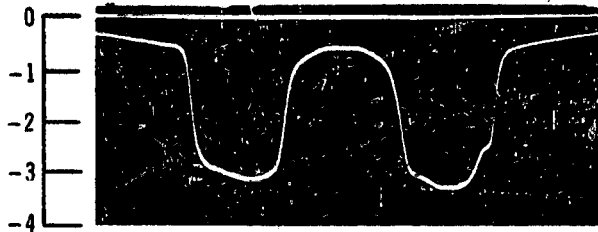
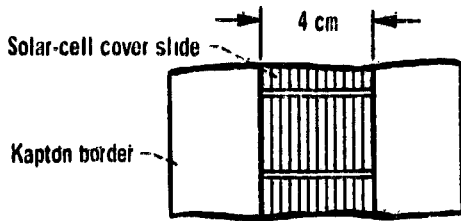


Back surface
(c) Sample 3.

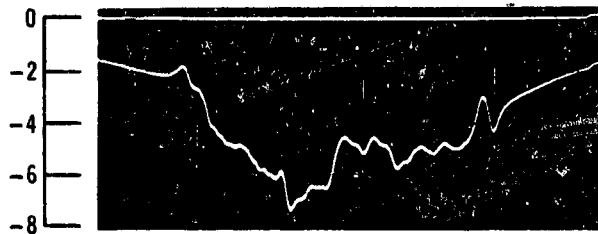


Back surface
(d) Sample 4.

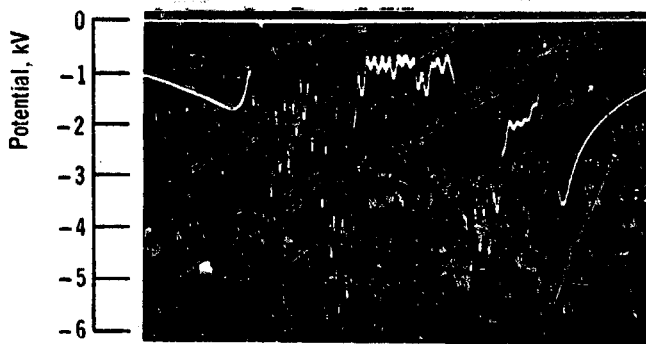
Figure 1. - Flexible-substrate solar-array samples.



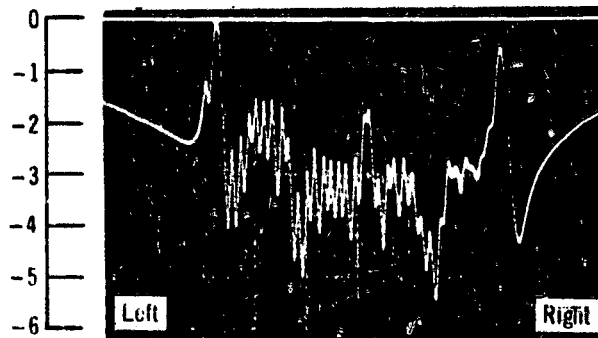
(a) Front surface: 5-keV beam; minute 26; 1 kV/division.



(b) Front surface: 20-keV beam; minute 20; 2 kV/division.



(c) Back surface: 20-keV beam; minute 1; 1 kV/division.



(d) Back surface: 20-keV beam; minute 20; 1 kV/division.

Figure 2. - Typical surface potential profiles of sample 2.

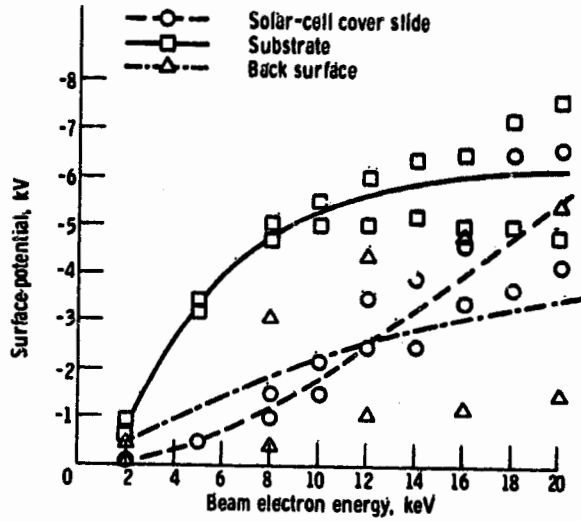


Figure 3. - Surface potential as function of beam energy for sample 2.

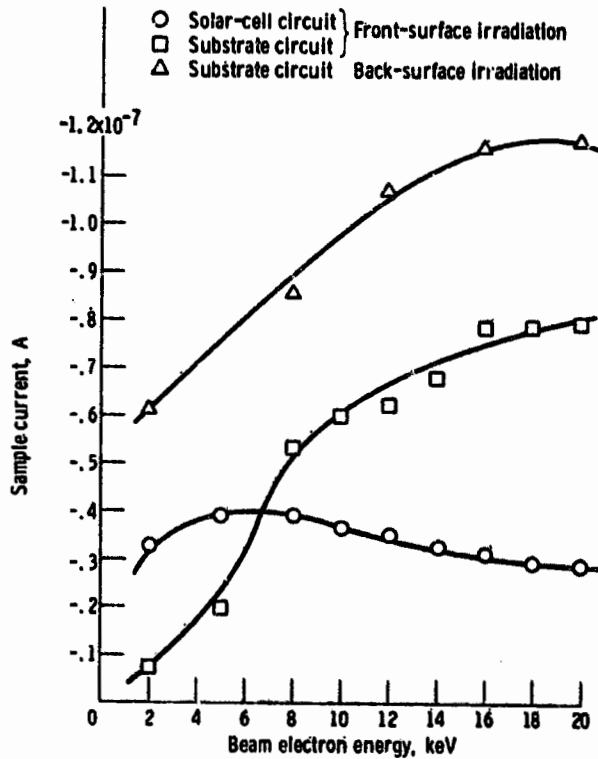


Figure 4. - Collected current as function of beam energy for sample 2.

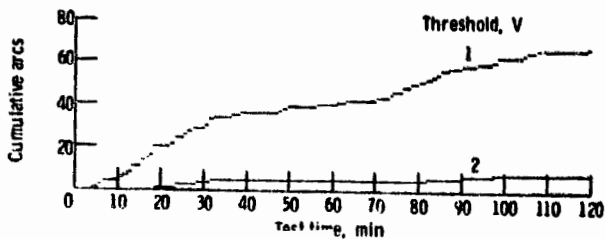
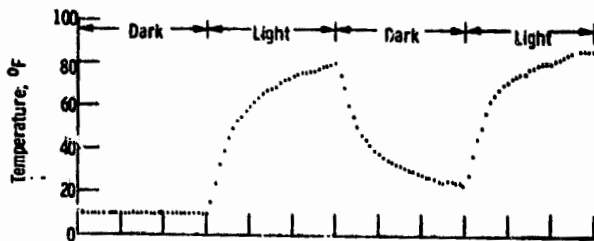
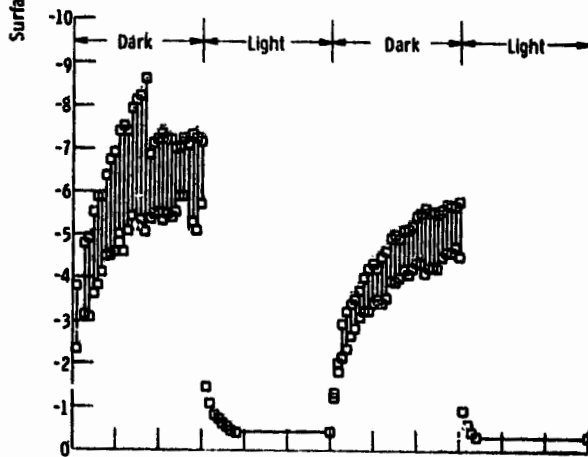
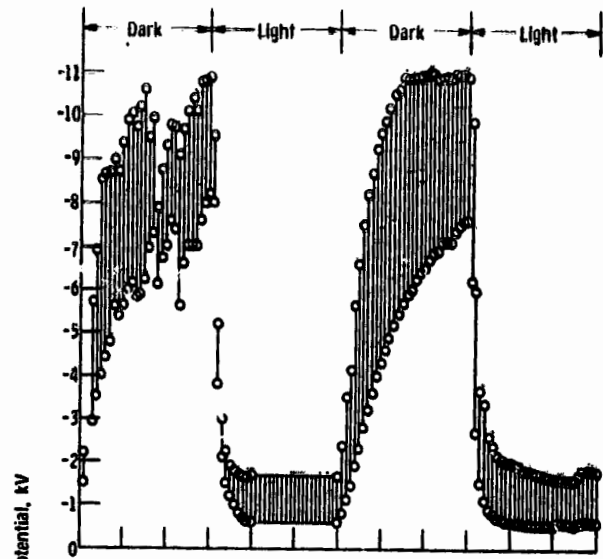
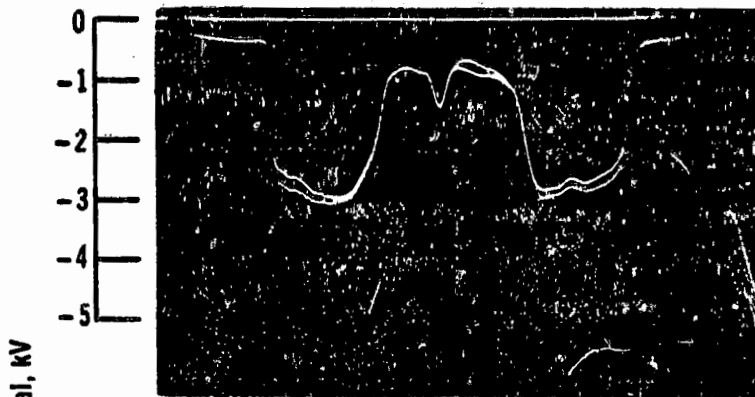
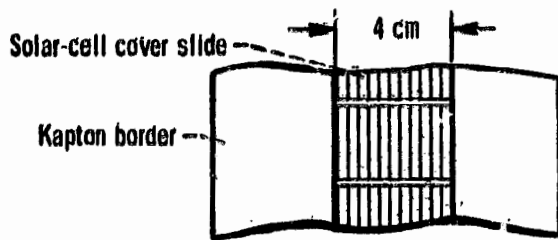
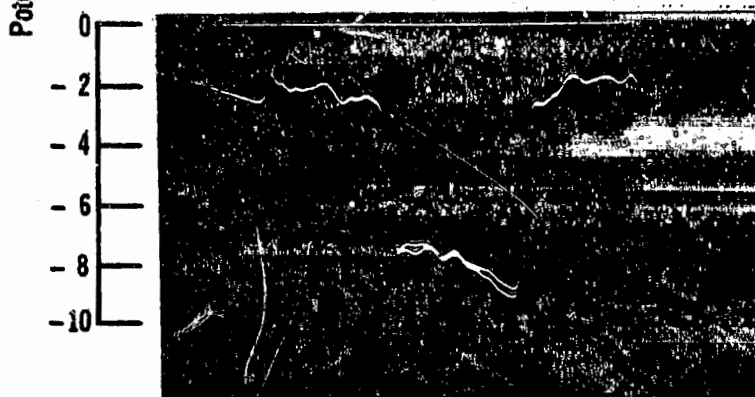


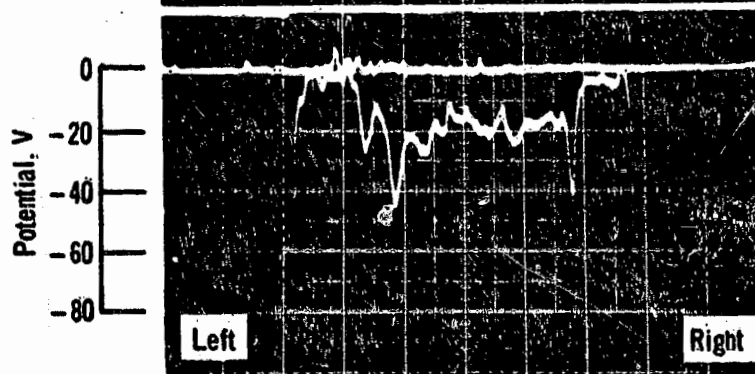
Figure 5. - Results of solar simulation test of sample 2.



(a) Front surface: 5-keV beam; minutes 20 and 27; 1 kV/division.



(b) Front surface: 20-keV beam; minutes 15 and 20; 2 kV/division.



(c) Back surface: 20-keV beam; minute 20; 20 V/division.

Figure 6. - Typical surface potential profiles of sample 3.

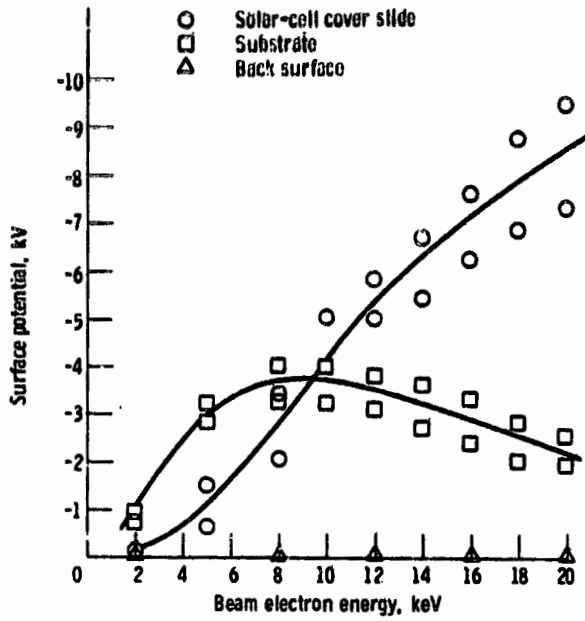


Figure 7. - Surface potential as function of beam energy for sample 3.

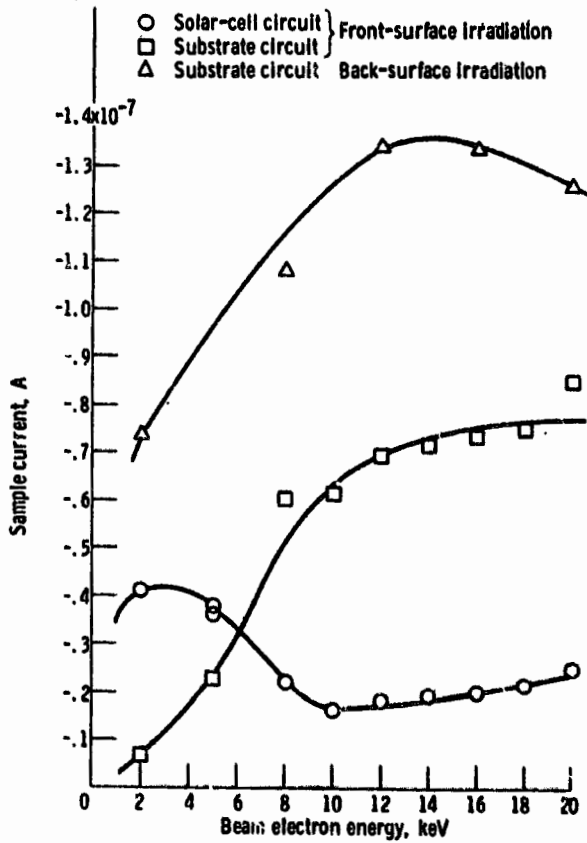
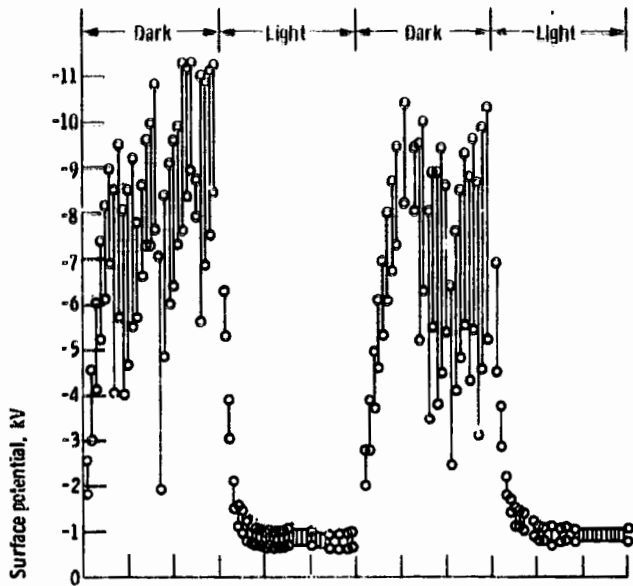
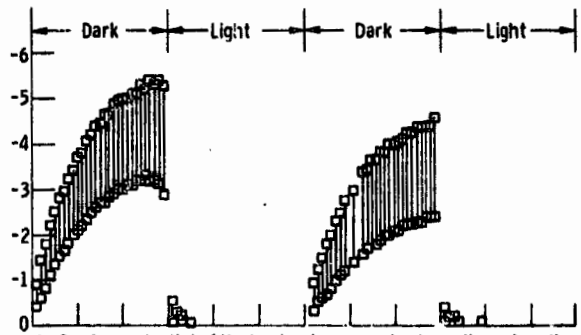


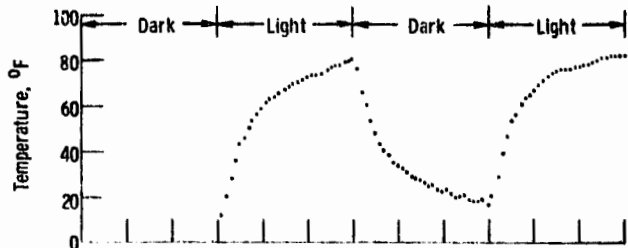
Figure 8. - Collected current as function of beam energy for sample 3.



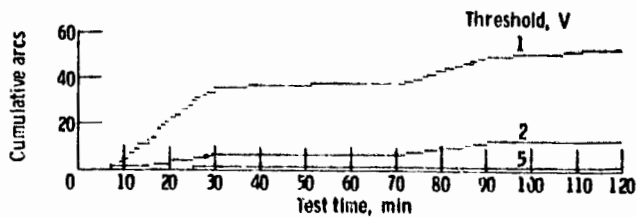
(a) Surface potential of solar-cell cover slides as function of time.



(b) Surface potential of Kapton border around solar cells as function of time.

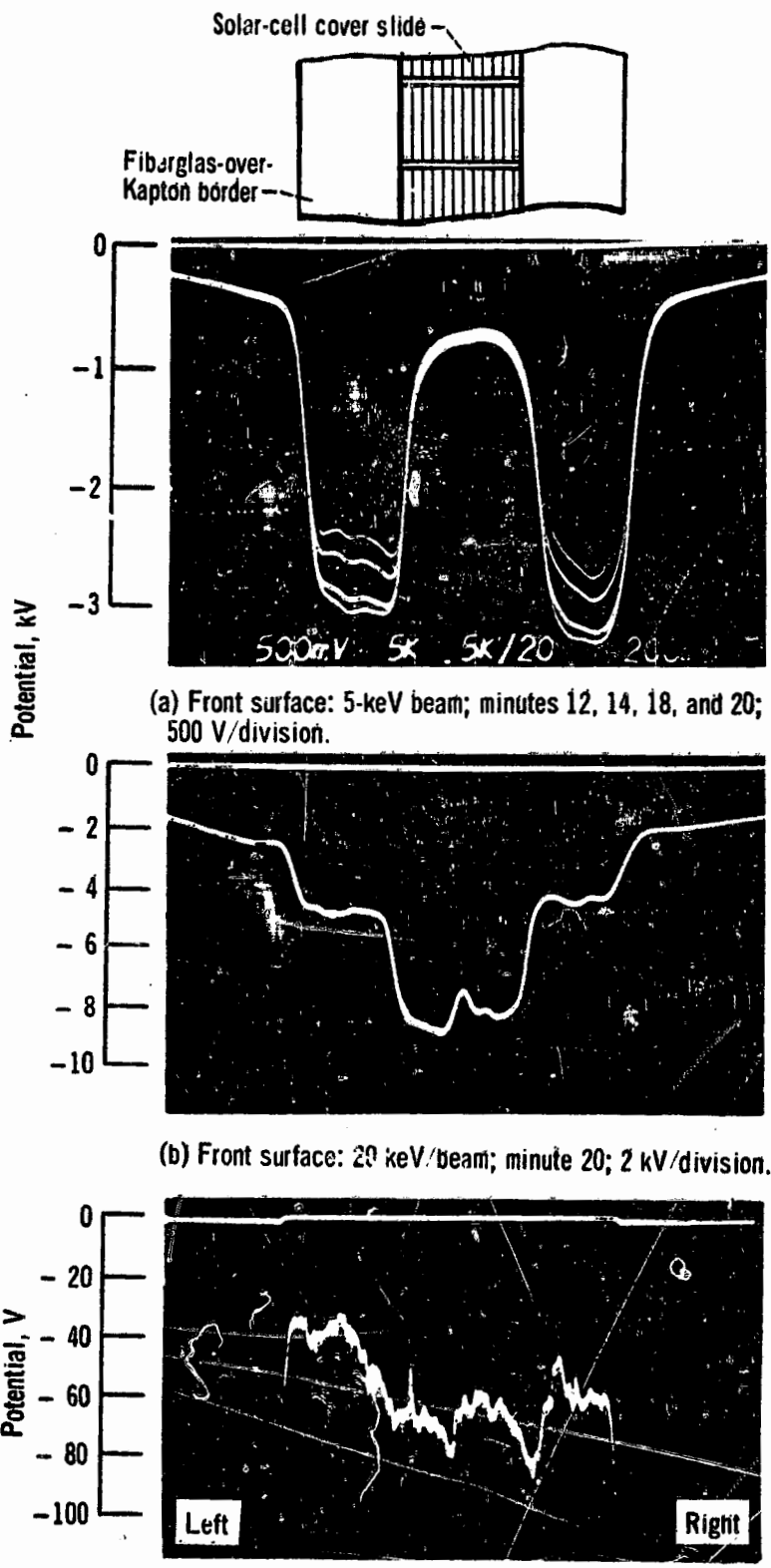


(c) Back-surface temperature as function of time.



(d) Cumulative discharge count as function of time.

Figure 9. - Results of solar simulation test of sample 3.



(a) Front surface: 5-keV beam; minutes 12, 14, 18, and 20; 500 V/division.
 (b) Front surface: 20 keV/beam; minute 20; 2 kV/division.
 (c) Back surface: 20-keV beam; minute 22; 20 V/division.
 Figure 10. - Typical surface potential profiles of sample 4.

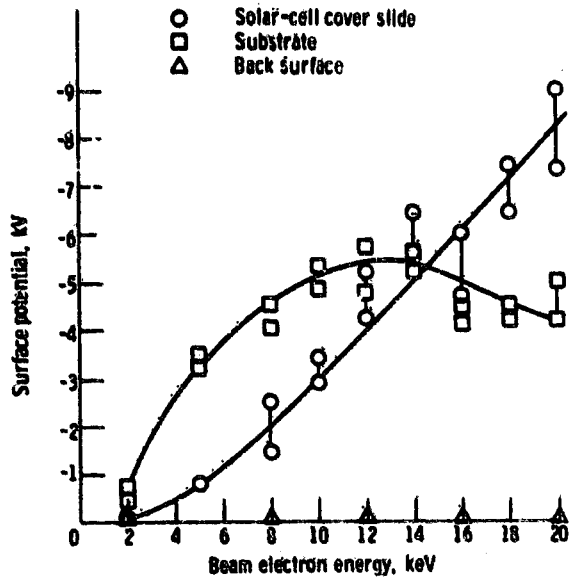


Figure 11. - Surface potential as function of beam energy — for sample 4.

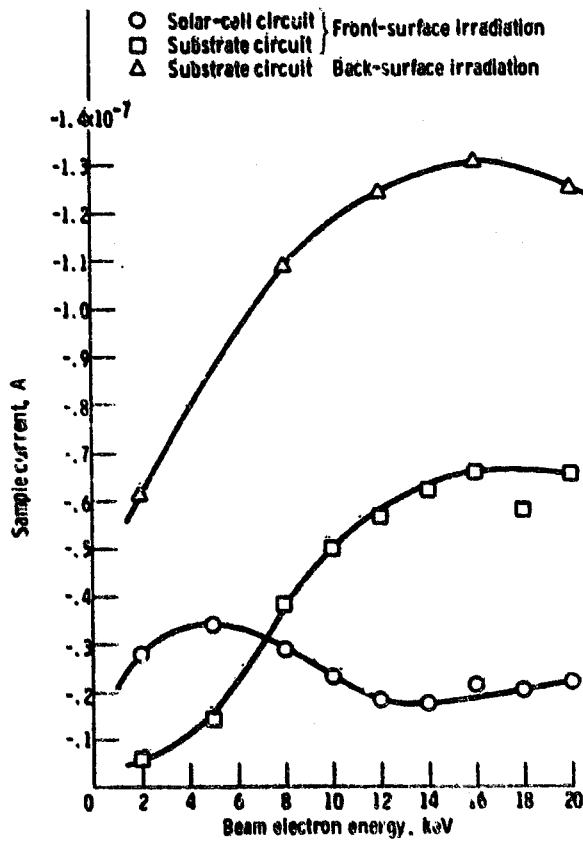


Figure 12. - Collected current as function of beam energy for sample 4.

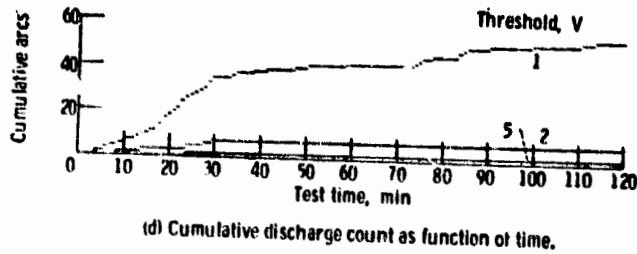
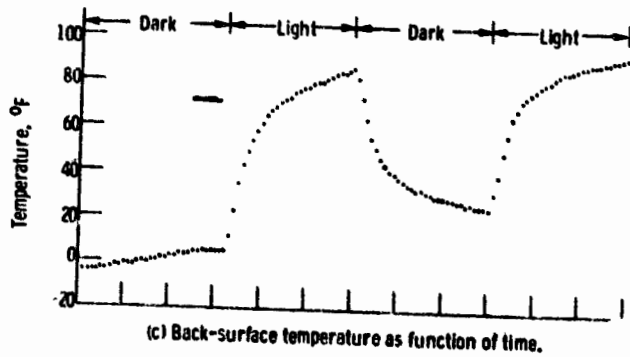
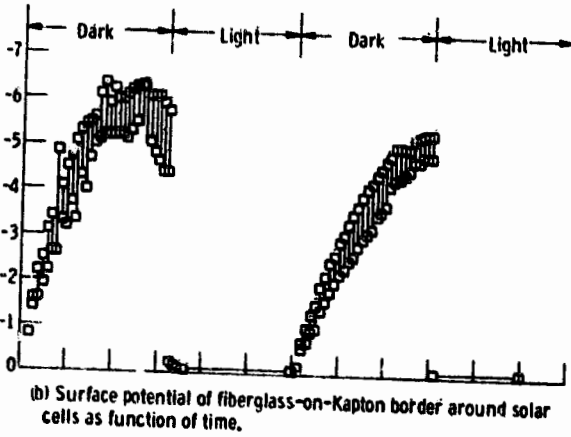
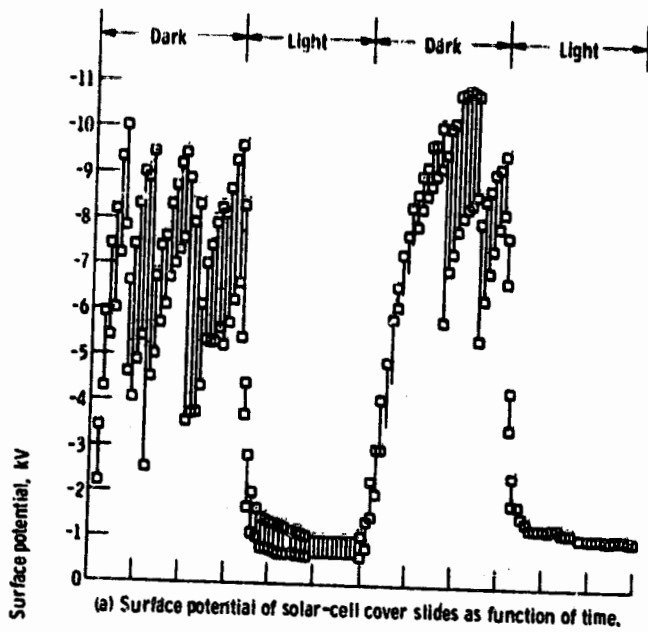
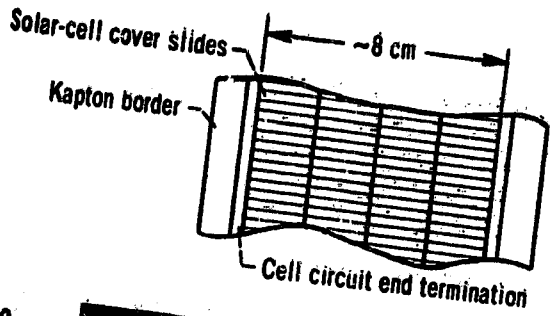
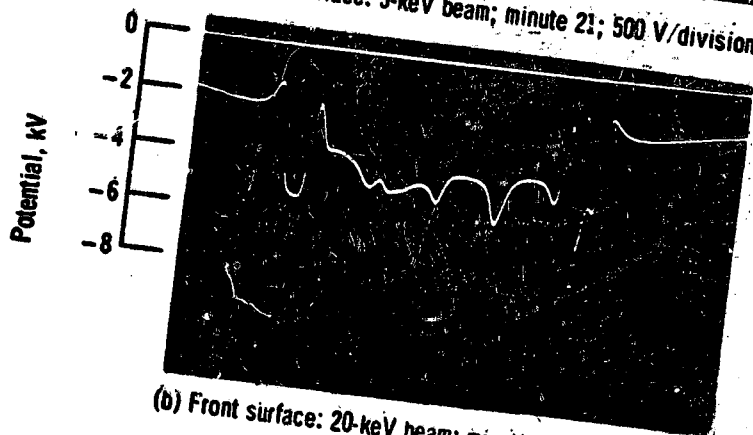


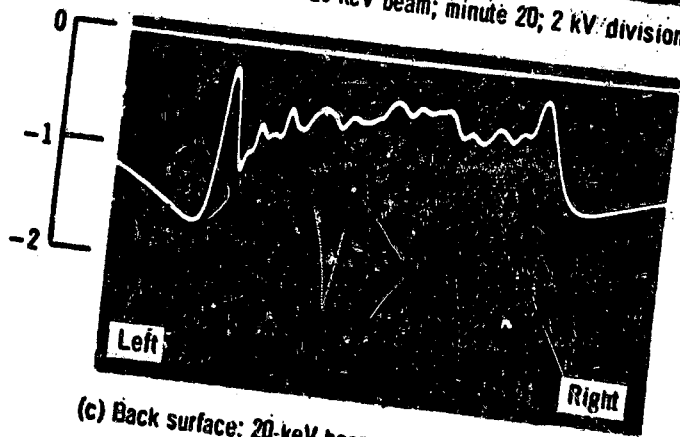
Figure 13. - Results of solar simulation test of sample 4.



(a) Front surface: 5-keV beam; minute 21; 500 V/division.



(b) Front surface: 20-keV beam; minute 20; 2 kV/division.



(c) Back surface: 20-keV beam; minute 30; 500 V/division.

Figure 14.- Typical surface potential profiles of sample 1.

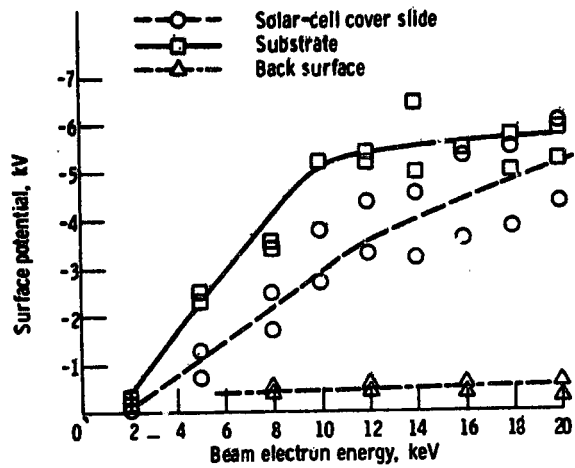


Figure 15. - Surface potential as function of beam energy for sample 1.

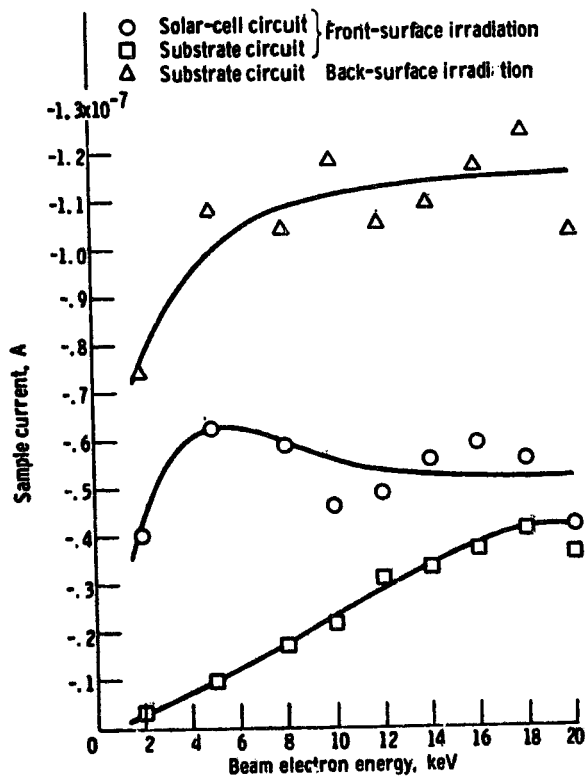


Figure 16. - Collected current as function of beam energy for sample 1.

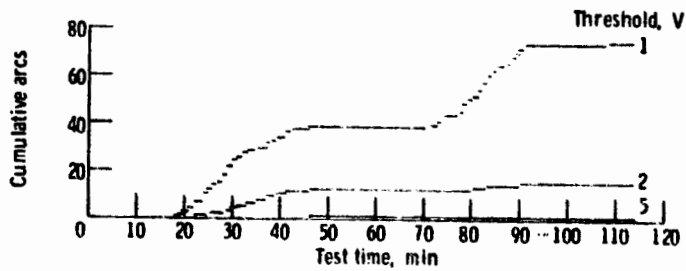
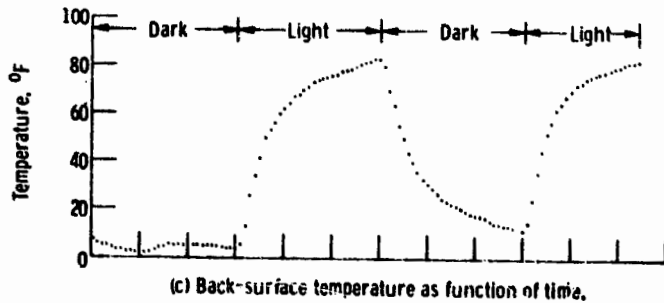
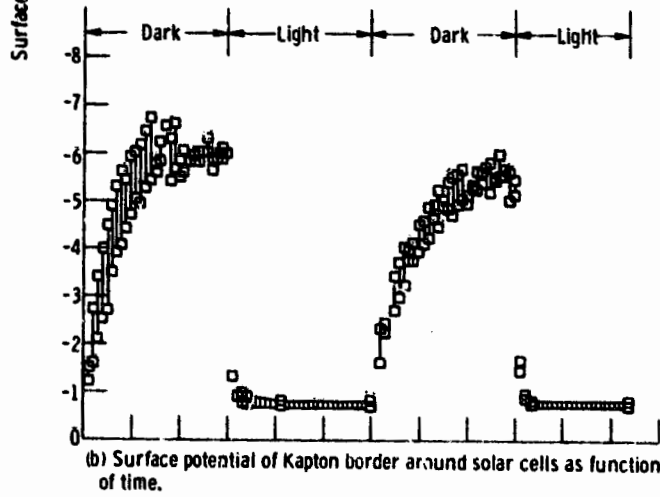
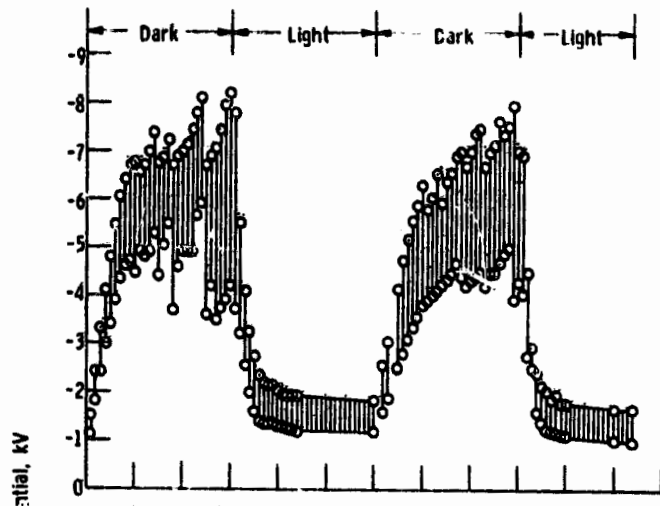
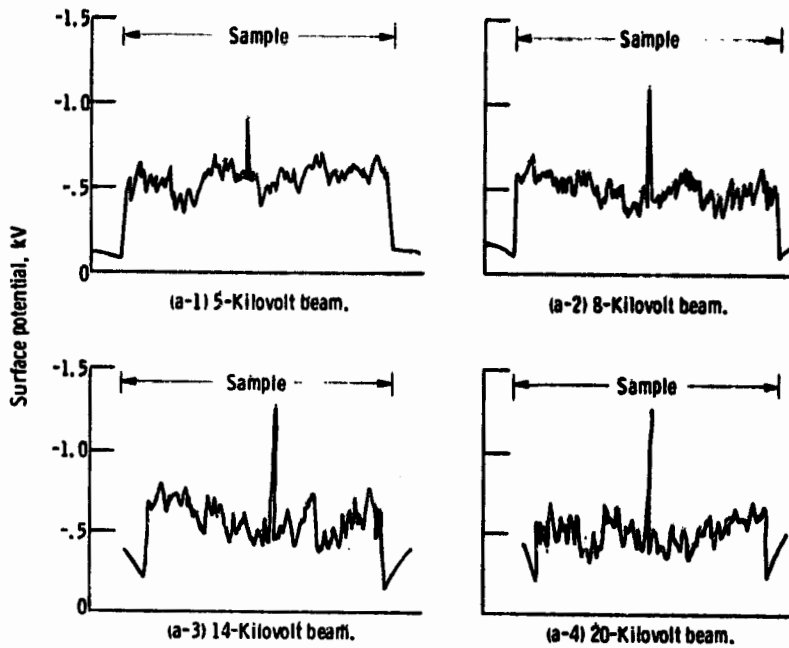
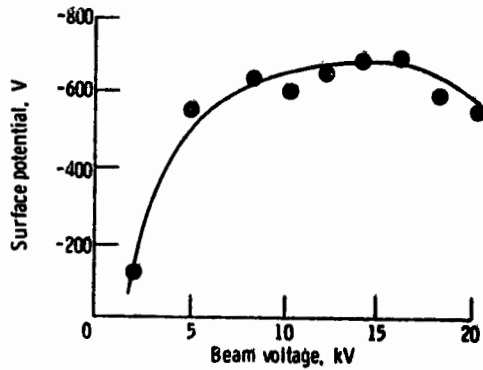


Figure 17. - Results of solar simulation test of sample 1.

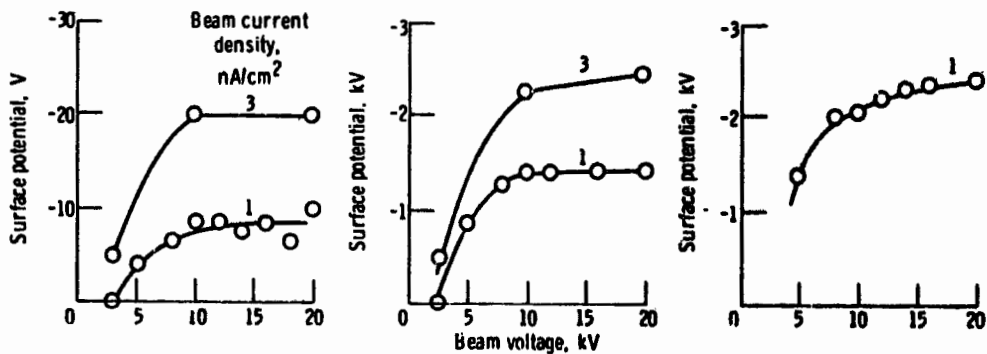


(a) Typical surface potential profiles.



(b) Equilibrium surface potentials in 1-nA/cm^2 -current-density electron beam.

Figure 18. - Results of Navstar solar-array substrate (sample 5) charging test.

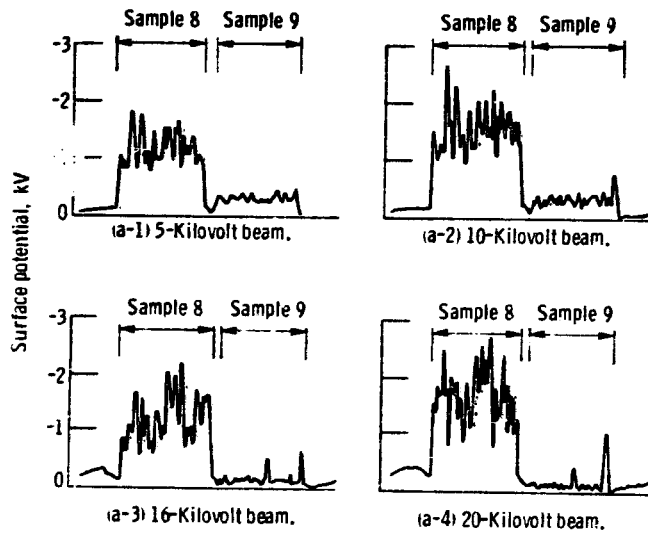


(a) Voyager antenna honeycomb panel with GSFC NS43C conductive paint (sample 6).

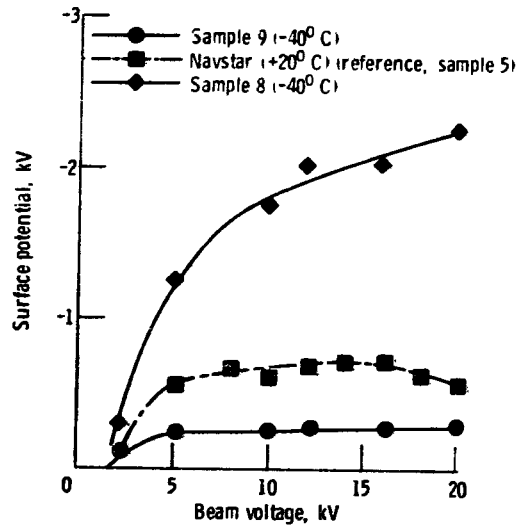
(b) Voyager antenna honeycomb panel with PV100 nonconductive paint (sample 7).

(c) Nonconductive paint (S-136LO) on grounded metal substrate for comparison.

Figure 19. - Results of Voyager antenna honeycomb-panel charging test.

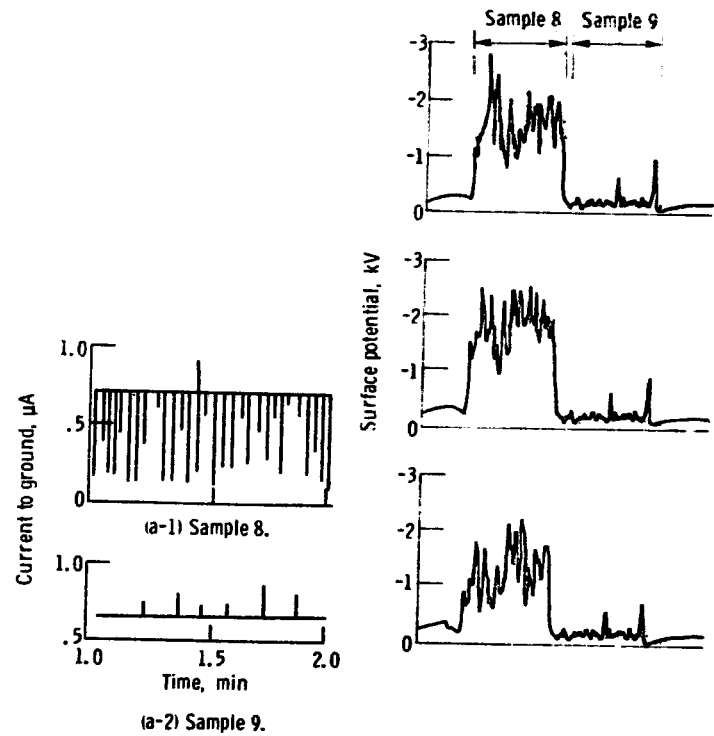


(a) Typical surface potential profiles.



(b) Equilibrium surface potentials for 1- and 3-nA/cm²-current-density electron beams.

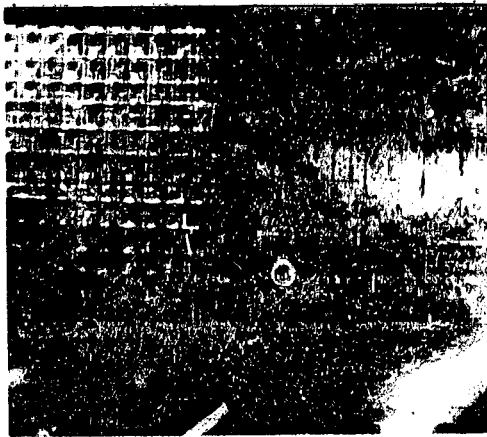
Figure 20. - Results of honeycomb-panel samples (8 and 9) charging tests.



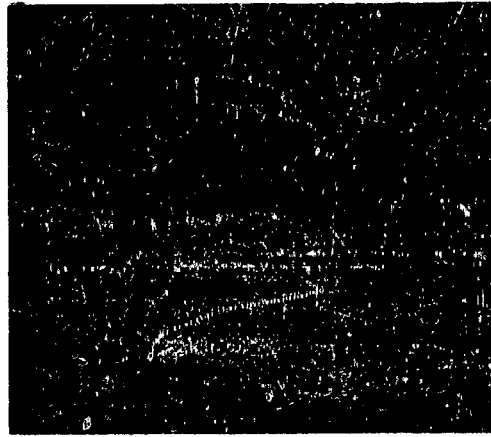
(a) Sample current traces in 16-keV electron beam.

(b) Surface potential profiles in 16-keV electron beam.

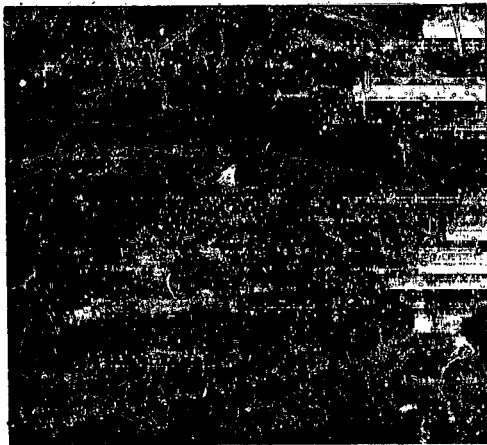
Figure 21. - Transient behavior of honeycomb-panel samples (8 and 9).



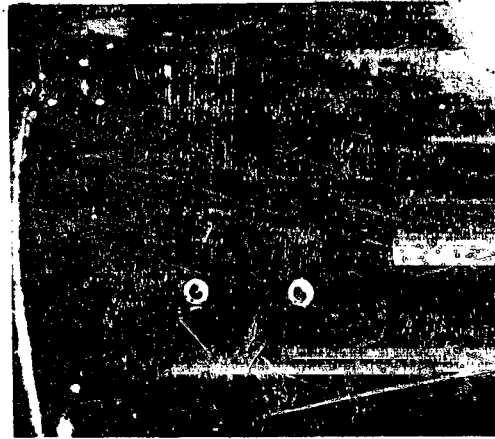
(a) 63-Minute time exposure at 16 keV; 1-nA/cm² electron beam.



(b) 10-Minute time exposure at 16 keV; 1-nA/cm² electron beam.



(c) Control time-exposure filament on, accelerating potential off.



(d) Surface voltage probe sweeping across top of sample 8.

Figure 22. - Time-exposure photographs of honeycomb panels (samples 8 and 9).

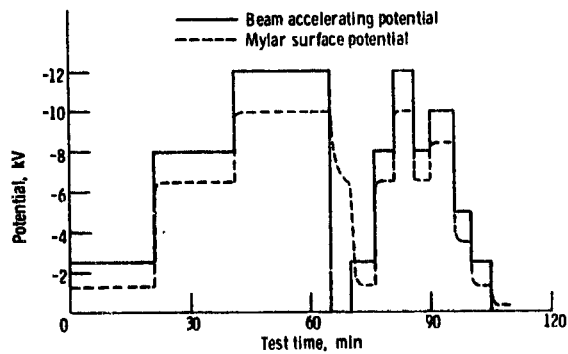


Figure 23. - Response of 2.54-micrometer-thick Mylar surface potential to varying electron beam energy. (Mylar isolated from ground.)

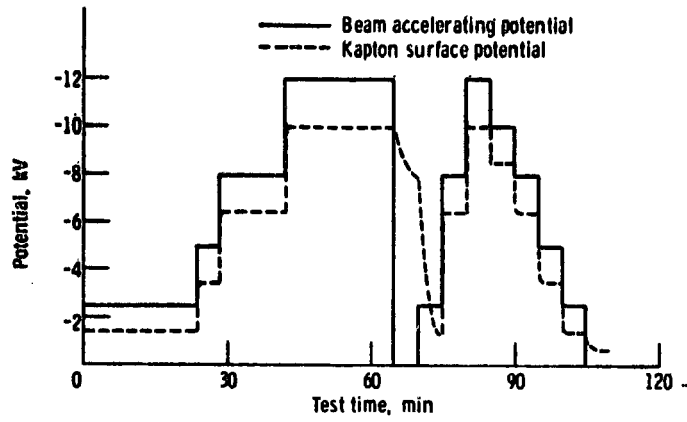


Figure 24. - Response of 7.62-micrometer-thick Kapton surface potential to varying electron beam energy. (Kapton isolated from ground.)

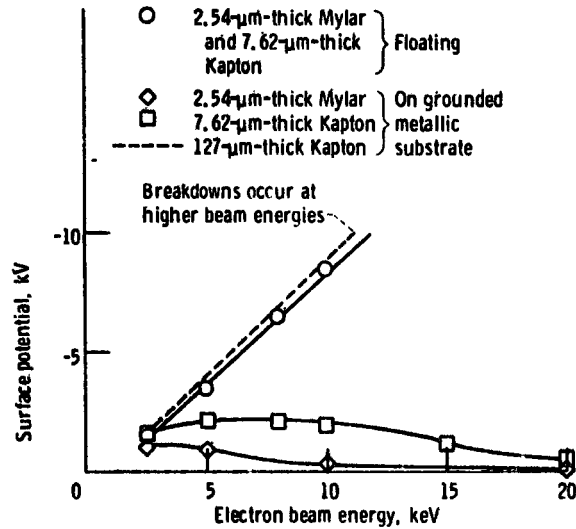


Figure 25. - Thin-film surface potential as function of electron beam energy.